PROGRESS IN PHOTOVOLTAICS: RESEARCH AND APPLICATIONS
Prog. Photovolt. Res. Appl. **6**, 151–161 (1998)

Research

Activation Energy of Local Currents in Solar Cells Measured by Thermal Methods

I. Konovalov,[1,*] V. Strikha[2] and O. Breitenstein[1]
[1]*Max Planck Institute of Microstructure Physics, Weinberg 2, D-06120 Halle, Germany*
[2]*Shevchenko University, Radiophysical Faculty, Volodymyrska 64, UA-252033 Kiev-33, Ukraine*

A new technique based on dynamic precision contact thermal measurements of the local current density of solar cells in the dark was developed to determine and map the activation energy of local currents. Because the activation energy or, more generally, the temperature dependence of the current density at constant bias in the dark is determined by the conduction mechanism, measurements of the activation energy may help to distinguish between various possible conduction mechanisms dominating in different regions of the cell. An application of this technique to multicrystalline silicon solar cells is presented. © 1998 John Wiley & Sons, Ltd.

INTRODUCTION

The efficiency of solar cells is determined by three parameters: the short circuit current, the open-circuit voltage and the fill factor. The open-circuit voltage and the fill factor strongly depend on the shape of the forward dark I–V characteristic of the cell. It is known[1] that the distribution of the forward current density over the whole cell area is often inhomogeneous. If the current density through a certain region of the cell is above the average, this inhomogeneity is called a 'shunt'. Thus, forward-bias shunt hunting is an important step in trying to increase the efficiency of solar cells. Thermal methods designed for diagnostics problems with respect to the locally increased forward current density in photovoltaic solar cells enabled us to map the forward current density distribution (dynamic precision contact thermography, DPCT[1,2]) and to obtain local I–V characteristics via thermal measurements (local I–V characteristics measured thermally, LIVT[3,4]). Both techniques are based on the dynamic temperature measurement in the contact mode, in which, in the dark, the sample is fed with rectangular periodic bias pulses, and the alternative part of the local surface temperature is measured locally in the lock-in mode by a small thermistor. Dynamic precision contact thermography maps are obtained by scanning of the cell at a certain pulsed bias by a thermistor, whereby the temperature modulation amplitude values are displayed. A DPCT map approximates the spatial current density distribution.

In the LIVT technique, the sensor is kept at a certain site on the surface, but the bias pulse amplitude is varied and the measured temperature modulation amplitude is divided by the amplitude of the bias pulses. The result is proportional to the local current in a certain bias range. Local I–V characteristics help to

* Correspondence to: I. Konovalov, Max Planck Institute of Microstructure Physics, Weinberg 2, D-06120 Halle, Germany. E-mail: ikono@mpi-halle.mpg.de

Contract/grant sponsor: BMBF; Contract/grant number: 0329 743 B
Contract/grant sponsor: ISSEP; Contract/grant number: PSU 072012

CCC 1062–7995/98/030151–11$17·50

Received 30 August 1997
Revised 21 November 1997

distinguish between different types of local inhomogeneities of the dark forward current density in solar cells. With the different bias dependencies of various conduction mechanisms, the LIVT technique yields information about the locally dominating conduction mechanism, i.e. the nature of a shunt. It is important to know the conduction mechanisms in order to learn how to avoid certain types of shunts. Nevertheless, sometimes the information from LIVT turns out to be insufficient to make conclusions about the current mechanism, in which case destructive investigations need to be carried out in order to check a certain hypothesis.[5,6] As will be shown below, activation energy studies performed by LIVT may yield additional information in a non-destructive way. We will call this new technique 'activation LIVT'. Investigating the temperature dependence of conventional I–V characteristics of the whole sample (I–V–T method) has become a common standard procedure for current mechanism studies (e.g. the study by Kaminski *et al.*[7]). Our technique enables this investigation to be carried out both locally and non-destructively.

For many forward current mechanisms in solar cells, the dark forward I–V curve can be presented as a function of temperature

$$I = Ai_s\left(e^{qV/nkT-1}\right) = Ai_0 \cdot e^{-E_a/kT} \cdot \left(e^{qV/nkT-1}\right) \tag{1}$$

where I is the current, A is the area, E_a is the activation energy, n is a parameter that in some cases is called the 'ideality factor' or simply 'n-factor', i_s is a prefactor of the current containing the activation energy, q is electron charge and V is the applied voltage. Here, i_0 may weakly depend on temperature, unlike the exponential term, or may be a constant. Sometimes i_0 is a function of the applied voltage. The physical meaning of the activation energy is straightforward whenever the current is proportional to the number of carriers able to climb an energy barrier of E_a and if the thermal energy of the carriers can be described by the Boltzmann law. The latter applies to non-degenerate semiconductors with the carriers thermodynamically not far from equilibrium. Indeed, these assumptions hold good for forward diffusion currents and currents due to recombination via deep impurity levels in the space charge region (SCR) in a p-n junction. They may also hold good for a forward current through an ideal Schottky barrier, where E_a can be interpreted as the junction barrier height. In a p-n junction, the local barrier height may decrease near grain boundaries.[8]

EXPERIMENTAL

The activation energy was measured using the standard DPCT instrument described in more detail in References 1 and 2. This instrument measures the sensor positioning, the application of the pulsed bias to the sample and the lock-in local AC temperature. The temperature of the sample holder is controlled by a HAAKE K20 refrigerator and a HAAKE DC3 digitally controlled thermostat. A temperature range of 15–40°C was chosen for the measurements. An increase in this range is possible but at higher temperatures the plastic film-cover begins to soften, and at temperatures lower than 15°C water condensation from the air is sometimes observed. Both effects affect the stability of the thermal contact between the sample and sensor, leading to an increased uncertainty in the results.

A special procedure was used for calibrating the sensitivity of the temperature measurement at all the temperatures used. A 2-mm wide and 100-μm thick nickel stripe served as a heat source of well-known properties when a predetermined current flowed through it. For calibrating the temperature measurement the nickel stripe was fed with a pulsed, stabilized current of 260 mA. The observed amplitude of sensor temperature modulation using the standard frequency of 3 Hz was of the order of 1 mK, which was two orders of magnitude above the noise level of the DPCT measurement technique. Taking into account the temperature dependence of the resistance of the stripe, we obtained calibration coefficients that allowed us to relate all results of the temperature measurements to the sensitivity of the equipment at a temperature of 25°C. Each current value of a LIVT measurement at a certain temperature was corrected by dividing it by the calibration coefficient. In Figure 1(a) the calibration coefficient is plotted as a function of temperature.

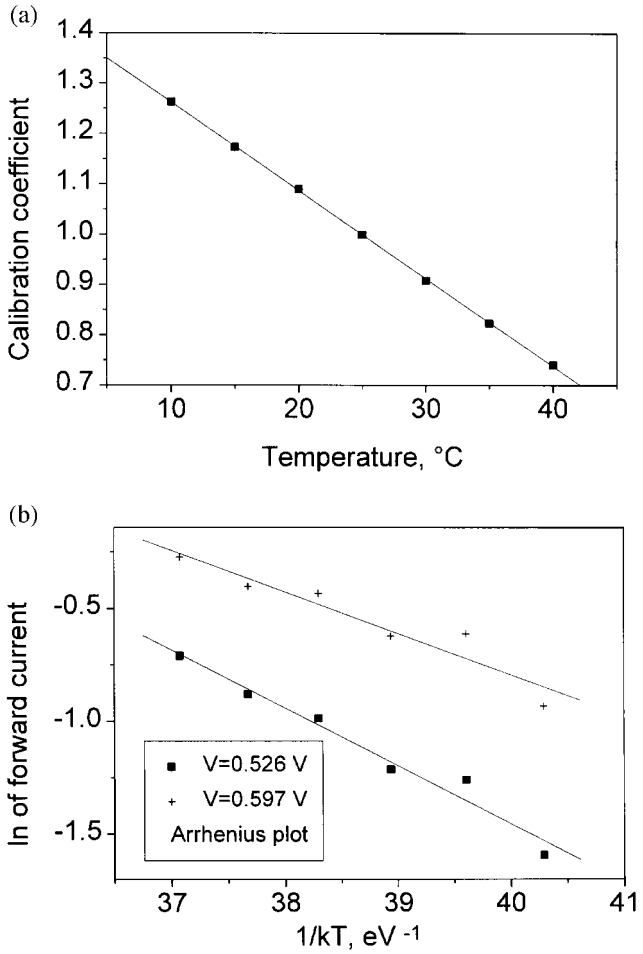

Figure 1. (a) Calibration coefficient as a function of the sample temperature; (b) Arrhenius plot: the $K(V)$ function is determined from its slope. These data correspond to the measurements referred to in Figure 3(a)

The usual procedure of determining the activation energy[7] includes three steps: exponential extrapolation of the series of forward I–V characteristics in semilogarithmic coordinates to zero voltage in order to determine the saturation current i_s; an Arrhenius plot of the saturation current; and from the slope of this plot the activation energy is determined. The first step presupposes the exponentially of the I–V characteristic, but this is not always met.[7]

This paper presents a special procedure for calculating the activation energy, taking into account, in general, a non-exponentiality of the local I–V characteristic. Here, for each voltage, the logarithms of the measured current values are fitted linearly as a function of $1/kT$ (Figure 1(b)) and, finally, the slope K of this fit is plotted as a function of voltage

$$\ln I = \ln(Ai_0) + \left(\frac{qV - nE_a}{nkT}\right) = \ln(Ai_0) - K(V)\frac{1}{kT} \tag{2}$$

$$K(V) = -\frac{qV - nE_a}{n} = E_a - \frac{qV}{n} \tag{3}$$

Extrapolation $K(V)$ to zero voltage yields the activation energy. Note that after the extrapolation the result does not depend on the value of the n-factor.

A similar technique can be used to map the activation energy of a solar cell. If two DPCT images are obtained for different temperatures but the same applied voltage, the map of the $E_a - qV/n$ parameter distribution can be obtained. If the calculation can be based on an n-factor map of the sample at the applied bias,[4] a map of the activation energy may be obtained. However, for solar cells, the sensitivity of state-of-the-art thermal mapping measurements allows us to determine the n-factor correctly only for regions of increased current density.

EXPERIMENTAL RESULTS AND DISCUSSION

Several types of inhomogeneities in n^+-p multicrystalline silicon solar cells were studied using this activation LIVT technique. Figures 2–5 present a series of LIVTs at various temperatures together with the functions $K(V)$. It should be noted that the series resistance always causes a sublinear behaviour of LIVTs at forward biases above 0.5 V. However, as a separate calculation shows, the error in E_a due to this influence, given in electron-volts, cannot exceed the apparent drop of voltage on the series resistance.

Non-defected regions far away from any shunts

Figure 2(a) presents the family of LIVTs of a 'normal' region of the cell far away enough from any shunt, whereas Figure 2(b) shows the function $K(V)$. The small amplitude of the signal outside the shunts resulted in a poor signal-to-noise ratio. An activation energy of $1{\cdot}1 \pm 0{\cdot}2$ eV (68% uncertainty) was obtained by extrapolating over the range 0·5–0·6 V. This is in good agreement with the energy gap E_g of silicon. Here, and below, the range for extrapolation was chosen so that the difference between the current at 15°C and at 40°C significantly exceeds the noise at the same voltage.

The deviation of $K(V)$ at lower voltages is due to the noise-induced measurement error, as follows from Figure 2(a). For the diffusion current flowing through an n^+-p junction at a low injection level, the forward current prefactor is[7,9]

$$i_{sn} = \frac{qn_p D_n}{l_n} \approx \frac{qn_i^2 D_n}{l_n N_a} - \sim T^3 \exp\left(-\frac{E_g}{kT}\right) \tag{4}$$

where i_{sn} is the saturation current of electrons, n_p, l_n and D_n are the concentration, the diffusion length and the diffusion coefficient of electrons in p-type material, respectively, N_a is the acceptor concentration and n_i is the intrinsic carrier concentration. If we neglect the relatively weak temperature dependence of the diffusion coefficient D_n and the diffusion length l_n, and if we suppose the hole concentration in the p-type material to be equal to the acceptor concentration N_a, then $E_a \approx E_g$ follows. A direct calculation showed that, under usual measurement conditions, the neglect of T^3 leads to a relative error in the current temperature dependence to within 10%.

Preferential conduction at grain boundary accumulations

Figure 3 illustrates the activation LIVT and $K(V)$ function of an extended shunt that occurred in a region where in electron beam-induced current a high density of electrically active grain boundaries was found. In Ref. 4 it was shown that this type of shunt shows spatial extensions of some millimetres and may react on mechanical stress in the wafer. The extrapolation of the $K(V)$ function of this shunt in the range 0·45–0·6 V results in an activation energy of 0·8 eV. This value was obtained in the region of I–V curve influenced by series resistance. The maximum apparent drop of voltage here is 0·065 V, which is the maximum possible error due to the series resistance. The experimentally obtained n-factor in the exponential region of the LIVTs in Figure 3(a) is 2·5.

The classical Shockley–Read–Hall theory of recombination currents in the symmetrical SCR via impurity levels in the midgap and with the same cross-sections to electrons and holes would lead to a

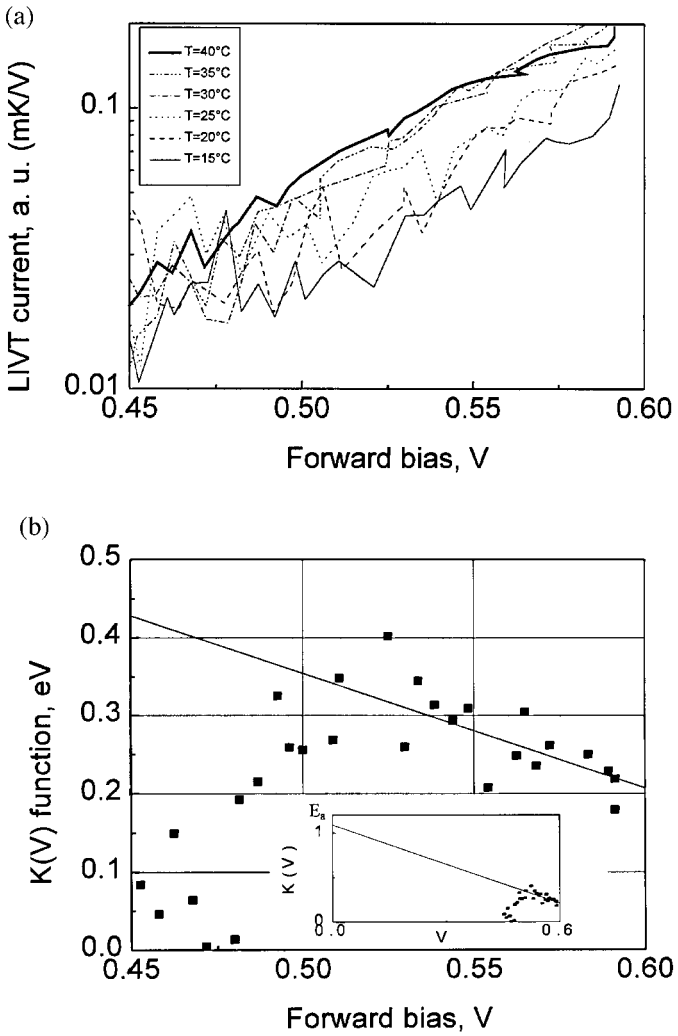

Figure 2. The series of temperature-activation LIVTs of a 'normal' (with no shunts around) region (a) and its function $K(V)$ (b) of a multicrystalline solar cell

forecast of $E_a \approx E_g/2 = 0{\cdot}56$ eV and an n-factor of Equation (1) of 2.[10] However, in Ref. 11 it was shown that, in general, both an n-factor exceeding 2 and an activation energy larger than half-bandgap may be explained in the case of an n^+-p junction by the recombination current mechanism if the saturation effects of several recombination centres in different locations in the bandgap are taken into account. Fitting the parameters of the theoretical model to experimentally obtained I–V curves resulted in an activation energy of 0·67 eV in Ref 11. This value was there confirmed also by a direct activation energy measurement. The activation energy shift is explained in Ref. 11 by a respective shift of the recombination level from the midgap. However, according to Ref. 11 an exponential I–V characteristic with $n > 2$ over an extended bias range requires the assumption of a rather specific-level distribution in the energy gap.

In Ref. 8 an alternative theory, not related to recombination in the SCR, was proposed. If the edge of a wafer crosses p-n junction, the potential barrier height of the junction may decrease locally. The reason for this generally bias-dependent decrease of the barrier height is the charging of a number of defect levels with trapped majority carriers, resulting in the formation of a surface depletion layer. This depletion layer forms a potential groove for minority carriers along the surface. Therefore, the local barrier height for injection via the p-n junction into this groove decreases locally. A similar effect is also possible at a grain

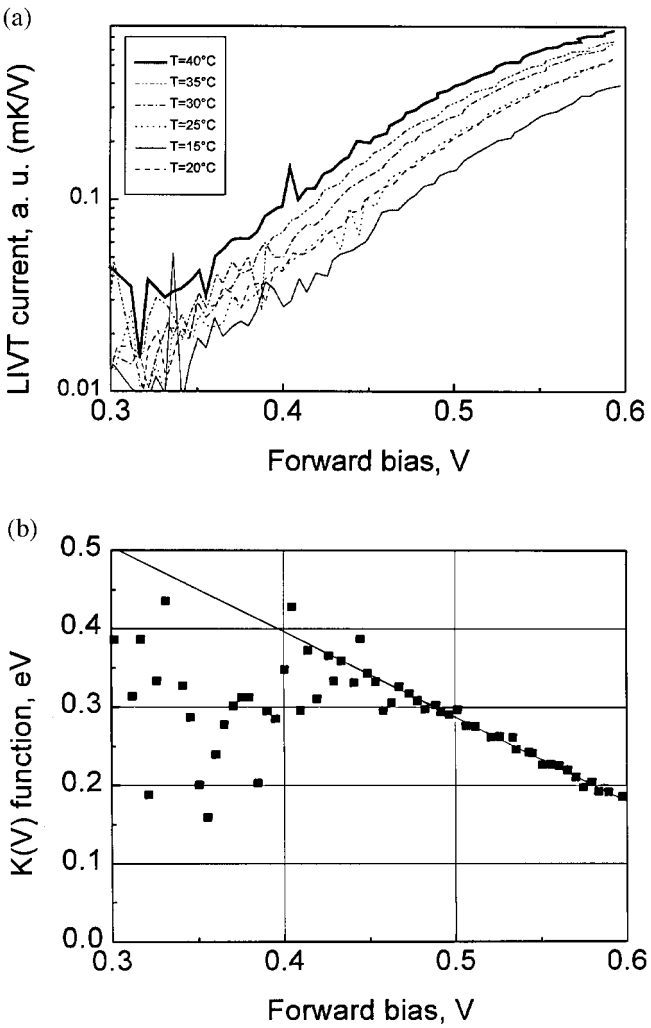

Figure 3. The series of temperature activation LIVTs of a shunt at an accumulation of electrically active grain boundaries (a) and its function $K(V)$ (b) of a multicrystalline solar cell

boundary crossing a p-n junction. Thus, at the sites where many grain boundaries cross the p-n junction, an increased forward current density is expected. This mechanism may also yield n-factors well above 2. The activation energy in this case might be expected to be less than E_g. Unfortunately, the activation energy study did not allow us to distinguish clearly this preferred potential groove injection from the recombination in the SCR mechanism.

Metal–semiconductor contact

Point-like shunts under grid lines were also investigated. They occurred always under metal grid lines and most probably arose from an occasional direct contact between the metal top grid and the p-type silicon bulk at sites of a damaged emitter layer under the metal contact. One of these shunts, the nature of which was afterwards proven by electron beam-induced current (EBIC) and scanning electron microscopy (SEM) investigations to be due to mechanical damage (scratch) of the textured silicon surface after the emitter formation (similar to that observed in Ref. 13), was used for activation energy measurements. The activation LIVT and the $K(V)$ function are presented in Figure 4. An apparent increase of the current from LIVTs near $V = 0$ is a measurement error induced by noise. The $K(V)$ function was extrapolated

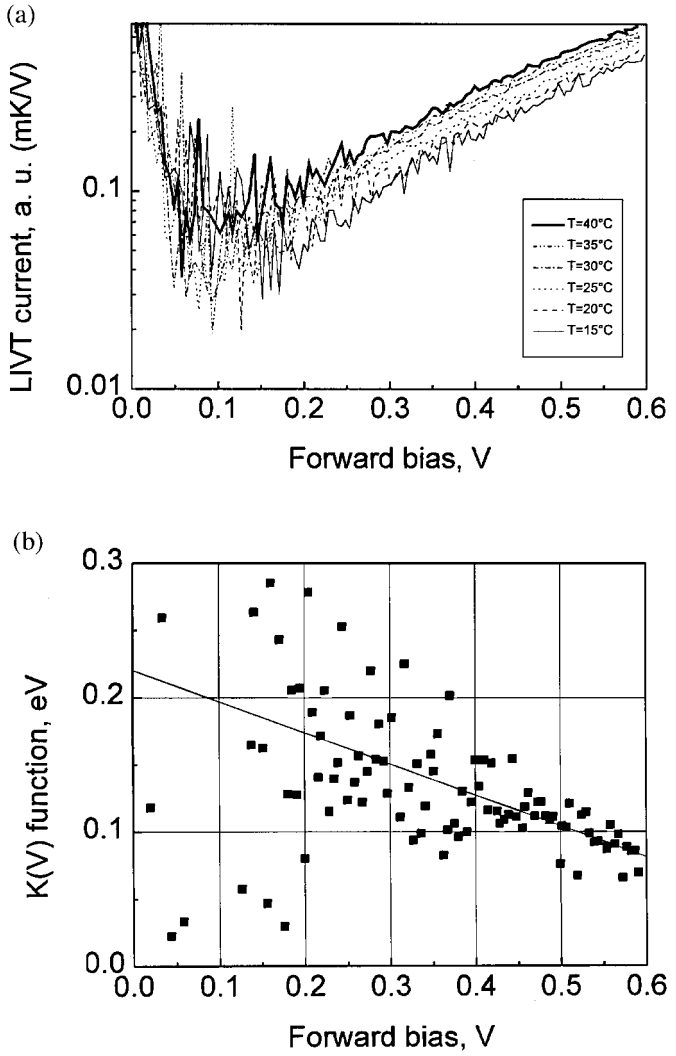

Figure 4. The series of temperature-activation LIVTs of a point-like shunt under a metal grid line (a) and its function $K(V)$ (b)

over 0·2–0·6 V, yielding an activation energy of about $0{\cdot}22 \pm 0{\cdot}02$ eV. Measuring the n-factor according to Figure 4(a) resulted in a value of about 7.

Several theoretical models of this inhomogeneity were considered. Tunnelling through the SCR of the Schottky barrier is less probable if the low doping level of p-type bulk material is considered. Surface trap-assisted currents may prevail only if an assumed insulating interlayer is sufficiently thin.[10] The observed behaviour may be interpreted using the following diffusion current model. According to Ref. 10, the forward current of the Schottky contact for a diode model with an insulating interface layer of tunnelling probability for holes R_p can be described as

$$\begin{aligned} I &= Ai_s\left[\exp\left(\frac{qV_2}{kT}\right) - \exp\left(-\frac{qV_1}{kT}\right)\right] \approx Ai_s \exp\left(\frac{qV_2}{kT}\right) \\ i_s &= \frac{qv_p R_p N_a}{4} \exp\left(-\frac{\varphi_0}{kT}\right) \\ V_1 + V_2 &= V \end{aligned} \tag{5}$$

where φ_0 is the barrier height at zero bias, N_a is the acceptor concentration, v_p is the thermal velocity of holes and V_1 and V_2 are fractions of the applied bias V, which drop on the insulating layer and on the SCR of the semiconductor, respectively. The n-factor is therefore determined by the fraction V/V_2 and, in general, can weakly depend on the applied bias V. Indeed, in Figure 4(a) a slightly sublinear behaviour is observed over the whole bias range. A measured n-factor of about 7 points to a relatively thick interface insulating layer between metal and semiconductor, because only about one-seventh of the applied voltage drops on the SCR in semiconductor; the rest of the bias drops on the interface layer between semiconductor and metal. The activation energy according to this model describes the barrier height φ_0. For a low-barrier Schottky contact, a barrier height of 0·22 eV seems reasonable.

Ohmic shunts

The last type of shunt investigated was the ohmic shunt. The LIVTs of ohmic shunts are linear, always showing the same slope in both polarities. Thus, I–V characteristics are not longer exponential, and neither are the activation LIVTs (Figure 5(a)). Nevertheless, our calculation procedure based on Equation (1) may be applied, yielding an activation energy. In the range of 0·15–0·4 V the values of K

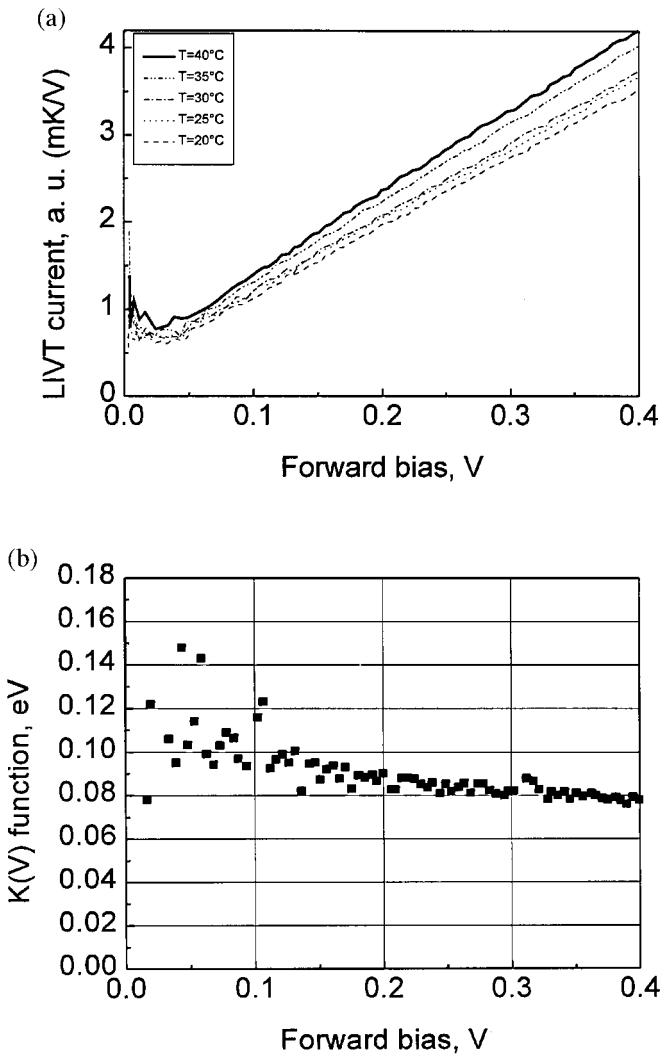

Figure 5. The series of temperature-activation LIVTs of an ohmic-type edge shunt (a) and its function $K(V)$ (b)

are almost constant (Figure 5(b)), which is expected from an ohmic shunt, the resistance of which does not depend on the bias. The activation energy from the extrapolated $K(0)$ value is $0{\cdot}08 \pm 0{\cdot}01$ eV, so the observed temperature resistance coefficient is negative.

According to our knowledge, no ohmic edge shunt structure model has been proven experimentally in solar cells except for the obvious top- and back-metallization short circuit.[6] Our negative temperature coefficient points to a semiconductor shunt mechanism (short circuit due to residuals of the emitter layer over the edge, etc.).

In order to find out the nature of ohmic shunts, SEM and EBIC images of an ohmic shunt region were obtained (Figure 6, left and right, respectively). During fabrication of the cell the emitter layer on the edge was opened mechanically by grinding out the edge between the bottom and the edge surfaces containing the emitter layer. Figure 6 presents a 45° tilted view of both the edge surface (closer to the left) and the bottom surface (closer to the right on the both images) simultaneously. The contrast and brightness of the EBIC image are chosen so that only the effective emitter layer is visible as bright contrast. We see that the edge of the wafer is very rough. At the indicated position, the EBIC signal gradually decreases towards the bottom surface. This behaviour is expected from a shunt. Its beginning is connected to the emitter layer of the front surface, where the quantum efficiency is high. The second end is short-circuited to the bottom contact, resulting in no carrier collection. The scanning electron image shows that a certain part of the edge was broken out, obviously before the emitter formation. At the bottom of this region the emitter could not be opened by the grinding procedure, resulting in the shunt.

According to Ref. 12, the resistance of phosphorus-doped silicon decreases with increasing temperature due to scattering of carriers on charged impurities, if the phosphorus dopant concentration exceeds 10^{18} cm^{-3}. The emitter phosphorus concentration of the investigated cell clearly exceeded this value. Similar emitter layer residuals were observed at the other two ohmic shunt locations investigated.

Activation energy mapping

Figure 7 presents a DPCT map (a) and a map of $K(V) = E_a - qV/n$ (b) of another 10×10 cm^2 solar cell of the same type, both obtained at 0·5 V forward bias in the dark. The $K(V)$ map was obtained from two DPCT maps at 25°C and at 40°C. Bright regions in Figure 6(a) refer to regions of increased current density. Strong shunts on the circumference mostly have linear LIVTs. The positions of these shunts correlate with the dark contrast in map (b) corresponding to a low $K(V)$.

Most of the shunts within the cell area have a relatively high value of $K(V)$ close to half the bandgap, thus showing no distinct contrast in the activation map. However, three shunts show lower activation energies: one in the lower part (A) and two in the middle (B) and closer to the right (C). All these shunts

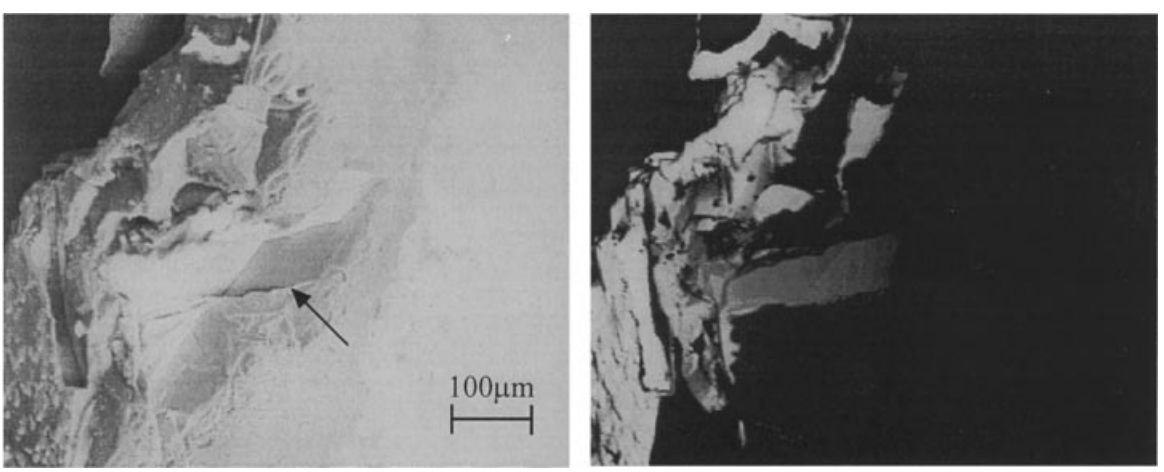

Figure 6. The SEM (left) and EBIC (right) images of an ohmic shunt

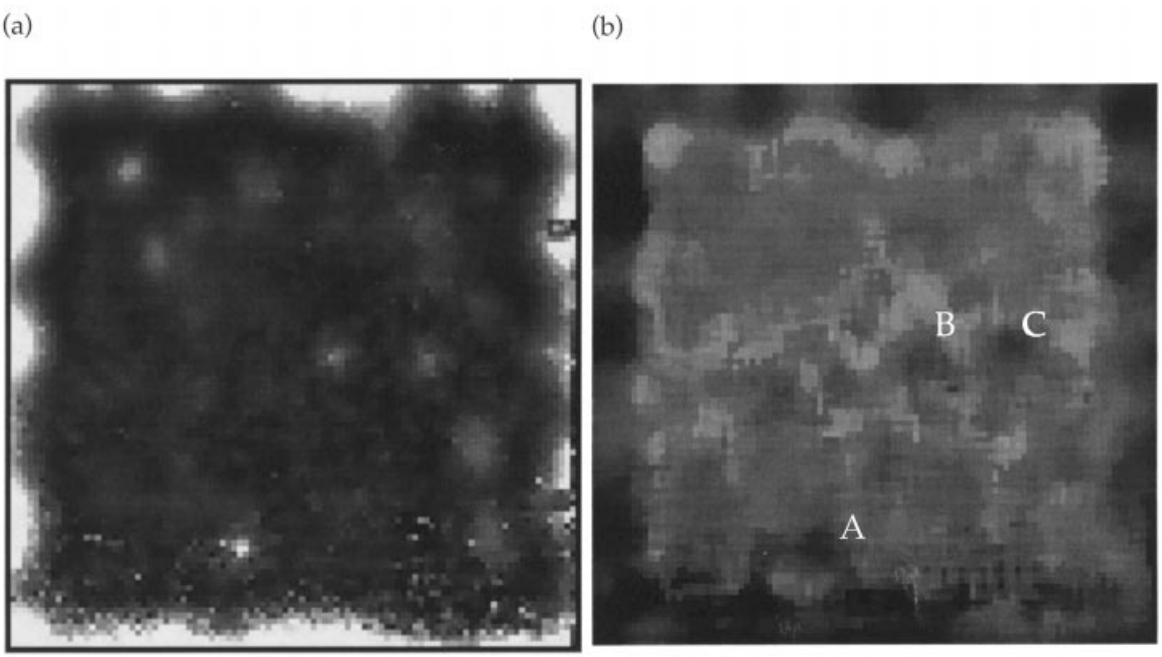

Figure 7. (a) A DPCT map (black: 0 mK, white: 0·15 mK temperature modulation at 25°C average temperature). (b) A DPCT map after noise reduction by smoothing of the $K(V) = E_a(-qV/n)$ (black: 0 eV, white: 1 eV) of a 10×10 cm^2 multicrystalline silicon solar cell

have fairly exponential forward LIVTs and are located between grid lines. The shunt closer to the bottom (A) shows a very high n-factor of 16, whereas that closer to the middle (B) has an n-factor of about 6. For these two shunts, we may suppose the map to represent adequately the low activation energy of these shunts. However, this does not apply to the shunt on the right (C), which has an n-factor of about 2·3 so that its activation energy is about 0·2 eV higher than the $K(V)$ value shown.

CONCLUSIONS

Studies of the LIVT temperature dependence have become possible. They feature a new non-destructive technique that yields fundamental information about locally dominating currents in solar cells. This information is additional to that of LIVT at constant temperature. The exact calibration of the precision temperature measurement equipment at various temperatures is necessary. It is realized by using test ohmic sources of known properties. The special procedure of data treatment allows one to gain the activation energy of shunts by not assuming their I–V characteristic to be exponential. The activation energy mapping was also shown to describe degraded areas of solar cells. However, one should be careful in mapping shunts with a low n-factor, because the mapping does not take into account the bias dependence of the barrier height. The application of this technique to multicrystalline solar cells is in agreement with existing models of shunt mechanisms. The activation study allowed certain shunt parameters, such as the barrier height in a Schottky contact model of a point-like shunt under the grid line, to be evaluated.

Acknowledgements

This work was supported by the BMBF under contract no. 0329 743 B and, in part, by the International Soros Science Education Program (ISSEP) through grant no. PSU 072012.

REFERENCES

1. O. Breitenstein, W. Eberhardt and K. Iwig, 'Imaging the local forward current density of solar cells by dynamical precision contact thermography', *Proc. 1st World Conference on Photovoltaic Energy Conversion, Hawaii*, 1994, pp. 1633–1636.
2. O. Breitenstein, K. Iwig and I. Konovalov, 'Evaluation of local electrical parameters of solar cells by dynamic (lock-in) thermography', *Phys. Status Solidi A*, **160**, 271–282 (1997).
3. I. Konovalov, O. Breitenstein and K. Iwig, 'Dynamical precision contact thermography (DPCT) and non-destructive local *I–V* measurements on solar cells', *Proc. 23rd ICPS, Berlin*, 1996, Vol. **4**, pp. 3243–3246.
4. I. Konovalov, O. Breitenstein and K. Iwig, 'Local current–voltage curves measured thermally (LIVT): a new technique of characterizing PV cells', *Sol. Energy Mater. Sol. Cells*, **48**, 53–60 (1997).
5. A. Simo and S. Martinuzzi, *Hot spots and heavily dislocated regions in multicrystalline silicon cells', Proc. 21st IEEE PVSC*, 1990, pp. 800–805.
6. O. Breitenstein and K. Iwig, 'Forward bias shunt hunting in solar cells by dynamical precision contact thermography', *Proc. 13th European Photovoltaic Solar Energy Conf.*, 1995, pp. 145–149.
7. A. Kaminski, J. J., Marchand, H. El Omari and A. Laugier, *Conduction processes in silicon solar cells', Proc. 25th IEEE PVSC*, 1996, pp. 573–576.
8. O. Breitenstein and J. Heydenreich, 'Non-ideal *I–V* characteristics of block-cast silicon solar cells', *Solid State Phenom.*, **37/38**, 139–144 (1994).
9. S. M. Sze, *Physics of Semiconductor Devices*, 2nd Edn, Wiley, New York, 1981.
10. V. I. Strikha, *Contact Phenomena in Semiconductors*, Vystshaja Shkola, Kiev, 1982 (in Russian).
11. J. Beier and B. Voß, 'Humps in dark *I–V* curves — analysis and explanation', *Proc. 23rd IEEE PVSC*, Louisville, 1993, pp. 321–326.
12. W. C. O'Mara, R. B. Herring and L. P. Hunt (eds), *Handbook of Semiconductor Silicon Technology*, Noyes Publications, New Jersey, 1990.
13. O. Breitenstein, K. Iwig and I. Konovalov, 'Identification of factors reducing V_{oc} in MC silicon solar cells', *Proc. 25th IEEE PVSC*, Washington, 1996, pp. 453–456.

